

# Image Analysis and Modeling in Ophthalmology

Edited by

E. Y. K. Ng

U. Rajendra Acharya

Aurélio Campilho

Jasjit S. Suri



CRC Press

Taylor & Francis Group

Boca Raton London New York

---

CRC Press is an imprint of the  
Taylor & Francis Group, an **informa** business

MATLAB® is a trademark of The MathWorks, Inc. and is used with permission. The MathWorks does not warrant the accuracy of the text or exercises in this book. This book's use or discussion of MATLAB® software or related products does not constitute endorsement or sponsorship by The MathWorks of a particular pedagogical approach or particular use of the MATLAB® software.

CRC Press  
Taylor & Francis Group  
6000 Broken Sound Parkway NW, Suite 300  
Boca Raton, FL 33487-2742

© 2014 by Taylor & Francis Group, LLC  
CRC Press is an imprint of Taylor & Francis Group, an Informa business

No claim to original U.S. Government works

Printed on acid-free paper  
Version Date: 20131108

International Standard Book Number-13: 978-1-4665-5930-1 (Hardback)

This book contains information obtained from authentic and highly regarded sources. Reasonable efforts have been made to publish reliable data and information, but the author and publisher cannot assume responsibility for the validity of all materials or the consequences of their use. The authors and publishers have attempted to trace the copyright holders of all material reproduced in this publication and apologize to copyright holders if permission to publish in this form has not been obtained. If any copyright material has not been acknowledged please write and let us know so we may rectify in any future reprint.

Except as permitted under U.S. Copyright Law, no part of this book may be reprinted, reproduced, transmitted, or utilized in any form by any electronic, mechanical, or other means, now known or hereafter invented, including photocopying, microfilming, and recording, or in any information storage or retrieval system, without written permission from the publishers.

For permission to photocopy or use material electronically from this work, please access [www.copyright.com](http://www.copyright.com) (<http://www.copyright.com/>) or contact the Copyright Clearance Center, Inc. (CCC), 222 Rosewood Drive, Danvers, MA 01923, 978-750-8400. CCC is a not-for-profit organization that provides licenses and registration for a variety of users. For organizations that have been granted a photocopy license by the CCC, a separate system of payment has been arranged.

**Trademark Notice:** Product or corporate names may be trademarks or registered trademarks, and are used only for identification and explanation without intent to infringe.

**Visit the Taylor & Francis Web site at**  
**<http://www.taylorandfrancis.com>**

**and the CRC Press Web site at**  
**<http://www.crcpress.com>**

# 15

---

## *Modeling of Laser-Induced Thermal Damage to the Retina and the Cornea*

---

Mathieu Jean and Karl Schulmeister

### CONTENTS

15.1	Introduction .....	265
15.2	Beam Propagation in the Eye .....	266
15.3	Minimum Spot Size .....	267
15.4	Optical Models .....	268
15.4.1	Single Lens Approximation.....	268
15.4.2	Ray Tracing .....	269
15.4.3	Modulation Transfer Function.....	270
15.4.4	Practical Aspects.....	270
15.5	Ocular Transmission .....	271
15.6	Optical Properties of Ocular Tissues .....	272
15.6.1	Retina.....	272
15.6.1.1	Distribution of Absorbers and Layer Geometry .....	274
15.6.1.2	Regional Variations.....	275
15.6.1.3	Fundus Reflectance.....	275
15.6.2	Cornea .....	276
15.7	Heat Transfer .....	277
15.7.1	Heat Equation.....	277
15.7.2	Initial and Boundary Conditions .....	279
15.7.3	Solving the Bioheat Equation .....	280
15.7.4	Characteristic Results.....	280
15.8	Modeling of Damage.....	282
15.8.1	Lesion Definition.....	282
15.8.2	Mathematical Description .....	283
15.8.3	Lesion Size and Computation .....	286
	References.....	287

---

### 15.1 Introduction

The very properties that make laser radiation a valuable tool in many fields—namely its high intensity and collimation—are also the critical reasons for potential eye and skin hazards (Sliney and Freasier 1973; Henderson and Schulmeister 2001). In general, optical radiation—be it ultraviolet, visible light, or infrared—is absorbed in the superficial layers of the body due to its high water content (mostly relevant for infrared) and the various

pigments and chromophores it contains (mostly relevant in the ultraviolet and visible ranges). The absorbed energy can then be converted into a thermoelastic pressure wave and heat, and can even trigger chemical reactions. All these interactions can ultimately lead to tissue damage if injury thresholds are exceeded. Among all organs, the eye is by far the most sensitive as it combines several critical factors: (i) pigments and water-based constituents provide high absorption capacity, (ii) irradiance can be greatly increased as optical radiation is focused onto the retina, and (iii) a lesion is rarely reversible and can be severely impairing.

Exposure limits for laser-based applications are first set in guidelines by expert committees such as the International Commission on Non-Ionizing Radiation Protection (ICNIRP), then adopted by IEC 60825-1 on an international level or ANSI Z136 in the United States. These guidelines are based on experimentally determined levels of minimal injuries that—combined with an appropriate safety factor—correspond conceptually to an acceptable hazard level (known as maximum permissible exposure or exposure limit). The experimental basis consists of identifying just-discernible lesions ophthalmoscopically assessed in the hours following exposure under laboratory conditions (typically 1–48 h). The so-called minimum visible lesion (MVL) is the standard threshold in the field of laser safety. Rabbits and macaque monkeys usually serve as experimental models to provide threshold data for the human cornea and retina, respectively. However, given the time-consuming nature of the experiments as well as ethical and economical considerations, the experimental approach cannot solely provide all necessary information or encompass all potential exposures. Computer modeling therefore is an appealing complementary support for safety questions and for improving scientific knowledge of laser–tissue interactions.

In this chapter, we concentrate on the investigation of thermally induced threshold damage to the cornea and retina (discussion on photochemical and mechanical interactions can be found in, for instance, Glickman 2002). We describe the fundamentals of physics-based models intended for this specific laser–tissue interaction and for reproducing experimental threshold values. We briefly review the optics of the eye and the optics of layered tissues and discuss setting up the bioheat equation and modeling the occurrence of macroscopic damage.

---

## 15.2 Beam Propagation in the Eye

In principle, laser-induced threshold damage levels depend on three parameters: exposure duration, wavelength, and—as long as the damage mechanism is thermal in nature—the size of the irradiated area (or spot size). In the case of retinal exposure, exposure duration and intraocular power are known but the retinal spot size cannot be directly measured. Only the beam divergence and source size are systematically measured while the irradiance profile at the retina has to be predicted mathematically.

The optics of the eye has been extensively studied in recent decades and precise data on various ocular properties are available. However, a simple and accurate representation of the retinal image is not straightforward and is complicated by the fact that it depends on many anatomical factors specific to the involved subject: instantaneous refractive state, local ocular aberrations, eccentricity, intraocular inhomogeneities, pupil size, and more (Milsom et al. 2006). Moreover, dynamic effects may play a crucial role: residual eye movements for long exposures or thermal lensing in the case of strongly attenuated

infrared-A (IR-A) wavelengths (780–1400 nm, due to high irradiance levels within the lens in Maxwellian view for instance; Vincelette et al. 2008). Nevertheless, all these phenomena tend to increase the power level required to induce a lesion, which implies that—when addressing the question of safety limits—only the worst cases must be predicted accurately.

---

### 15.3 Minimum Spot Size

Investigators in the field of laser-induced damage to the retina designate the radial extent of light absorption within the retina—and the following source term in the heat equation—as spot size. A major challenge lies in the determination of the *minimum* spot size. The determination of a characteristic lower limit to the focus of a collimated laser beam is crucial for setting safety guidelines (see discussion in Sliney 2005) since the threshold level varies with the square of the spot size for short exposures and linearly for longer ones. Yet, recent experimental results show strong evidence that thresholds do not further decrease for spot sizes below 70–100  $\mu\text{m}$  (i.e., beam divergence  $\sim 5$  mrad; Lund et al. 2007; Zuclich et al. 2008).

Attempts to achieve best-focused retinal spots show that the spot size can be reduced further on purpose in specific conditions; for example, by optimizing the beam positioning in order to avoid ocular inhomogeneities (Birngruber et al. 1979) or by using wave-front correction (Lund et al. 2008b). In an idealized aberration-free rhesus monkey eye, with a beam diameter at the cornea of, say 4 mm, and a laser wavelength of 590 nm, the diffraction-limited beam waist diameter approaches 3–4  $\mu\text{m}$ . Investigators have traditionally assumed that retinal diameters smaller than 20–30  $\mu\text{m}$  are not achievable in the typical conditions of laser-induced threshold lesion experiments (guidelines assume 25.5  $\mu\text{m}$  for the human eye), but for the purpose of modeling, this consensus is questioned and assumptions such as 60–70  $\mu\text{m}$  (Connolly et al. 1978) are more common (Welch et al. 1979; Lund et al. 2008a).

Only intraocular scattering is unlikely to enlarge the retinal spot size to such an extent since the postulated retinal image is approximately one order of magnitude above the limit of diffraction and smaller spots have been measured *in vivo* (Birngruber et al. 1979). However, scattering does reduce the part of energy contained in the central portion of the spot. For instance, if only 40% of the energy reaching the retina is efficiently focused (Birngruber et al. 1983), then additional input power is required in order to compensate for this loss. But in modeling, such widening of the retinal irradiance distribution is usually not directly modeled, but can be accounted for by defining an enlarged *effective* spot. As an attempt to account for the relative impact of scattering, an alternative can consist of considering a reduced spot-size-dependent ocular transmission (Jean and Schulmeister 2013).

Intraretinal scattering has also been suggested as a reason for augmenting the radial extent of light distribution at the retinal pigment epithelium (RPE) in the extrafoveal region (Welch et al. 1979; Schulmeister et al. 2006). Another possible explanation for the discrepancy between observed thresholds and model predictions in the minimal spot size regime involves limitations in the experimental detection techniques. According to this hypothesis, the absolute minimum lesions are not detectable by ophthalmoscopy and the ophthalmoscopically observed lesions are actually above threshold (Davis and Mautner 1969). Meanwhile, awaiting strong evidence of a reliable minimum spot size, the current

uncertainty necessitates safety factors between experimentally found thresholds and exposure limits to be of about 10 for collimated laser beams (Schulmeister et al. 2011).

## 15.4 Optical Models

### 15.4.1 Single Lens Approximation

Several investigators have shown that the retinal spot size can be measured *in vivo* using invasive techniques (Sanders 1974; Birngruber et al. 1979). In the case of extended sources, the following linear relationship between source size  $\theta$  and retinal spot size  $d$ ,  $d = \theta f$ , yields acceptable results (assuming a relaxed eye;  $\theta$  in milliradians,  $d$  and the focal length  $f$  in millimeters; see Figure 15.1a). Here the eye is considered as a single thin lens in air and in the paraxial approximation, source size and image size are linearly related. However, this does not hold for collimated beams. Moreover, it has to be considered that the focal length of an optical system depends on the wavelength of radiation, implying that chromatic dispersion can increase the spot size beyond its reference value. In the relaxed eye, a collimated beam reaches focus at the retinal plane for 590 nm (Atchison and Smith 2002; the helium  $d$  line at 587.6 nm is often used as a reference for estimating chromatic dispersion of materials such as in the Abbe value). A first refinement is thus to account for chromatic dispersion such as  $d(\lambda) = \theta f(\lambda)$  (Figure 15.1c). The wavelength-dependent focal

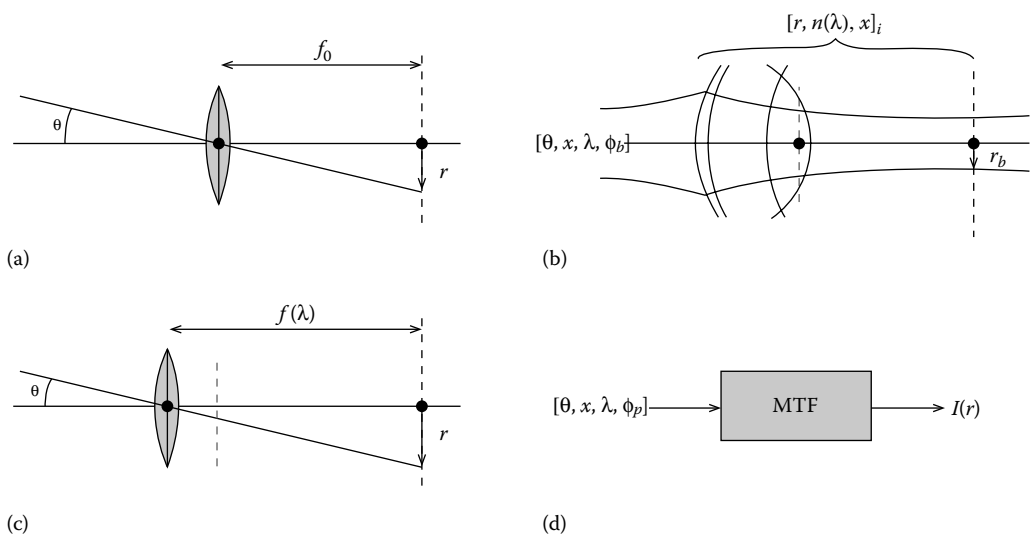


**FIGURE 15.1**

Review of optical models used in modeling of threshold damage to the retina ( $\theta$ , subtense angle;  $f$ , focal length;  $\lambda$ , wavelength;  $r_b$ , spot radius;  $x$ , position;  $\phi_p$ , beam diameter;  $\phi_p$ , pupil diameter;  $r$ , radius of curvature;  $n$ , index of refraction;  $I$ , intensity). (From (a) Henderson, R. and Schulmeister, K., *Laser Safety*, Taylor & Francis, New York, 2004. (b) Birngruber, R., Gabel, V.-P., and Hillenkamp, F., *Health Phys*, 44, 519–531, 1983. (c) Vincelette, R.L., Rockwell, B.A., Oliver, J.W., et al., *Laser Surg Med*, 41, 382–390, 2009. (d) Takata, A.N., Kuan, L.P., Goldfinch, L., Thomopoulos, N., Hinds, J.K., and Weigandt, A., Thermal model of laser-induced eye damage, USAF School of Aerospace Medicine, Brooks City-Base, TX, 1974.)

length is obtained from refractive error measurements and a wavelength of reference. The refractive error or chromatic difference of refraction can be expressed as:

$$R(\lambda) = \frac{1}{f_0} - \frac{1}{f(\lambda)}$$

The chromatic difference of refraction (in diopters) can be fitted by polynomials (Atchison and Smith 2005), thus obtaining a first estimate of the wavelength-dependent image size. This approach has been used, for instance, to extrapolate damage thresholds from one wavelength to others (this procedure is sometimes referred to as action spectrum, Lund et al. 2008a). The proposed dispersion equations slightly overestimate dispersion in the IR-A range (Vincelette et al. 2008). However, this representation still cannot provide a reliable measure of the retinal image in the case of either a collimated beam near best focus or varying iris apertures.

#### 15.4.2 Ray Tracing

Since the single thin lens approach is too coarse for representing the complexity of the eye, ray-tracing methods provide a finer view of more complex optical systems such as thick lenses. Basically, each ocular tissue—that is, cornea, aqueous chamber, lens, and vitreous—can be treated as a homogeneous medium delimited by two refractive surfaces, each having a given curvature. Their combination forms the schematic eye, whose primary task is to reproduce the optical properties of a system (see cardinal points) by adequately designing geometrical and optical properties: radii of curvature and spacing between surfaces, and indices of refraction, respectively (Figure 15.1b; more details in Atchison and Smith 2002).

Since chromatic aberration is the most dominant source of spot size variation—besides beam divergence—and because interindividual variations are minimized by the averaging effect of using several animals, a schematic eye is a convenient approach for including wavelength-dependent refractive indices. Formulae such as Cornu and Herzberger equations provide reasonable fitting of refractive error (the Herzberger equation is more appropriate in the IR-A range; Atchison and Smith 2005). Schematic eyes can also include complex properties such as asphericity, gradient refractive index, and eccentricity (e.g., tilt for modeling astigmatism).

A schematic eye is a useful basis for the application of ray transfer matrix analysis—also known as ABCD matrix analysis—where each component of the system is represented in a second-order matrix. In the paraxial approximation, both phenomena—propagation and refraction—are linear transformations of the input ray with respect to its angle:

$$\text{Propagation: } \begin{bmatrix} 1 & d \\ 0 & 1 \end{bmatrix} \quad \text{Refraction: } \begin{bmatrix} 1 & 0 \\ \frac{n_{in} - n_{out}}{R} & \frac{n_{in}}{n_{out}} \end{bmatrix}$$

where  $d$ ,  $n$ , and  $R$  stand for distance, index of refraction, and radius of curvature, respectively. Consequently, the combination of all optical elements is achieved by matrix multiplications.

$$M_{\text{eye}} = M_n \cdot M_{n-1} \cdot \dots \cdot M_0$$

For Gaussian beams, input and output rays are computed in the form of a basis vector incorporating the complex beam parameter. The image size can thus be calculated at any axial position. In ocular lesion experiments, lasers are often operated in the fundamental transversal mode in which the laser beam exhibits axial symmetry and its profile is described by a Gaussian function. This property is very convenient since a Gaussian profile remains Gaussian after transformation by an optical system. An in-depth discussion on ray transfer matrix analysis can be found in Gerrard and Burch (1994). Schematic eyes downscaled from human to monkey and ray-tracing methods have already been applied in laser-induced retinal damage modeling (e.g., Rockwell et al. 1997; Birngruber et al. 1983).

### 15.4.3 Modulation Transfer Function

The eye can be conceived as a linear and time-invariant system described by its modulation transfer function, that is, the Fourier transform of the point spread function (Figure 15.1d). This analytic method exhibits peculiar advantages, namely its validity for any source profile and the consideration of any kind of linear transformation, scattering, and attenuation (attenuation must be considered separately in geometrical optics). However, this method is not easily applicable in practice since the function needs to be measured at every single wavelength of the spectrum and requires a large number of subjects for averaging purposes. Consequently, this approach has not yet been used for retinal injury threshold modeling, but it is worth consideration for future efforts. An interesting way of formulating wavelength and eccentricity components is proposed by Hodgkinson et al. (1994).

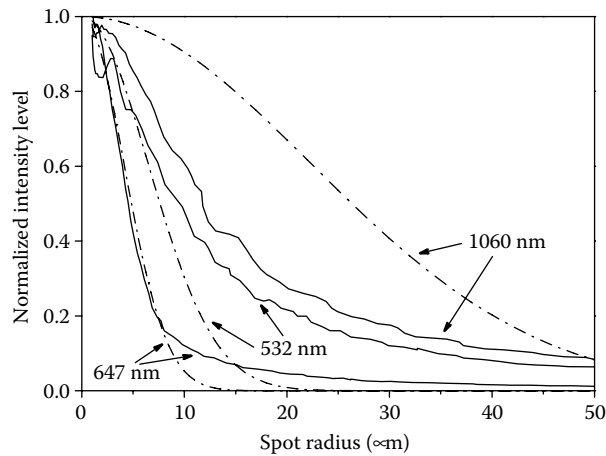
From scalar diffraction theory, especially in the Fresnel approximation, that is, near field, a formulation of the Fourier transform of the pupil can be obtained as a combination of aberration and defocusing phase functions. The near-field approximation is valid for all relevant values of pupil size and wavelength. Formulation and appropriate parameters have been developed by Takata et al. (1974).

### 15.4.4 Practical Aspects

A comparison of the results obtained by ray transfer matrix analysis and diffraction theory is shown in Figure 15.2 (applied by Jean and Schulmeister (2013) and Takata et al. (1974), respectively). As in laser-induced damage experiments, we consider the rhesus monkey eye in a relaxed state (after anesthetization) and fully dilated (pupil diameter 7 mm).

Aberrations of high order and diffraction by the pupil have a limited impact on spot size but they do modify the wide-angle irradiance profile on the retina. The one obtained from the diffraction theory has more pronounced tails than the Gaussian function assumed in ray tracing. This effect is also observed in the study of intraocular forward scattering, where energy is spread over a few degrees while the spot itself contains only 40%–50% of the transmitted intraocular energy (Birngruber et al. 1979). Even though there are some discrepancies, both models show to what extent the retinal spot size is affected by chromatic aberrations.

It should be mentioned that small-scale variations of the spot size—in the order of micrometers—have no direct effect on retinal damage levels for various reasons: (i) inter-individual and interlocation variations are randomly distributed, (ii) heat diffusion overcomes these irregularities within a few microseconds, that is, shorter than the thermal

**FIGURE 15.2**

Retinal intensity distribution at three wavelengths from two models: modulation transfer function (solid line) and ray tracing (dashed line).

damage regime, and (iii) damage is detected at a larger scale, that is, at least over a few tenths of micrometers (see Section 15.8). Consequently, light distribution at the retinal plane is commonly treated as a simple mathematical function (such as Gauss) and parameterized only by its diameter. Further refinements are thought not to be critical for the purpose of modeling retinal injury, except if minimum retinal spot sizes can be proven to be of the order of 10  $\mu\text{m}$  or smaller.

## 15.5 Ocular Transmission

A critical aspect is the degree of ocular transmission, which, in the range of 400–1400 nm, varies between practically 0% and 80%. This optical property is commonly obtained from *ex vivo* measurements (e.g., Boettner and Dankovic 1974). Two types of measurements are available, referred to as direct and total transmission. Transmitted light is distinguished into the part of collimated light (typically within  $1^\circ$ ) associated with direct transmission and the part of both collimated and diffuse light (i.e., within almost  $180^\circ$ ) associated with total transmission. We use these two types of characterization for representing ocular transmission for collimated beams and extended sources, respectively. However, no data are available for in-between cases. Attenuation is assumed to follow the Beer–Lambert law.

Above approximately 1150 nm, the eye filters optical radiation similarly to pure water (van den Berg and Spekreijse 1997) and transmission can be modeled well by considering a 19 mm equivalent path length of water for the young rhesus monkey eye (Bradley et al. 1999). At shorter wavelengths, the transmission spectra of water and those of all ocular tissues diverge significantly from each other. In the visible spectrum, the cornea exhibits the highest optical density while the lens and the cornea steeply cut off transmission below approximately 400 nm. Figure 15.3 shows the spectral optical density of the young rhesus monkey eye for both transmission types (direct and total) along with the pure water model. Attenuation is assumed to follow the Beer–Lambert law in both cases.

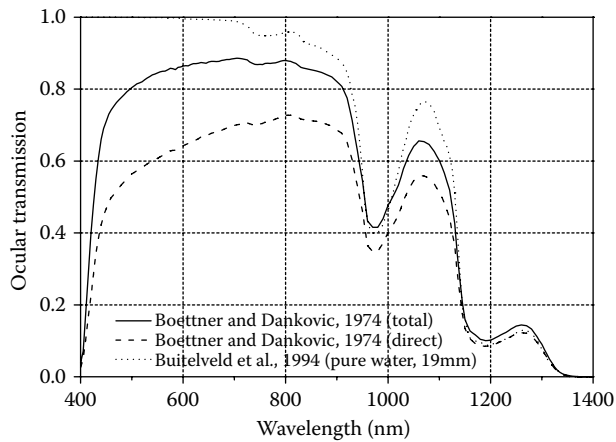


**FIGURE 15.3**  
Transmission of the rhesus monkey eye (solid and dashed lines) and of pure water (dotted line).

## 15.6 Optical Properties of Ocular Tissues

### 15.6.1 Retina

The sketch in Figure 15.4 schematically depicts a section of the retina. In principle, optical radiation strikes the back of the eye at the neural retina and to a large degree passes through the photoreceptors. The underlying layers—RPE, choriocapillaris, and choroid—are primarily devoted to anatomically and physiologically supporting the sensory organ, but they also play a determinant role in light absorption. A reasonable physiological

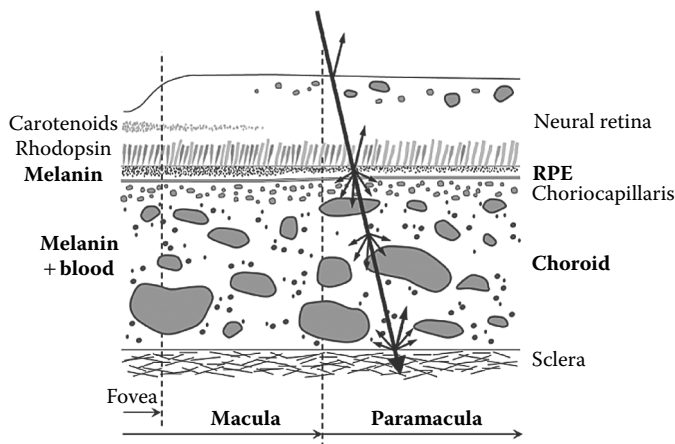


**FIGURE 15.4**  
Section of the primate retina with emphasis on pigments (labeled on the left) and the most relevant layers (labeled on the right). Idealized light paths are indicated (arrows). Retinal areas of importance are labeled at the bottom.

explanation is that the highly absorbing RPE layer eliminates backscattering, thereby improving image contrast. Furthermore, pigmentation of the RPE shields the cell nucleus from phototoxic UV radiation. A pernicious effect of the highly absorbing layer is that the retina becomes more vulnerable regarding thermal injury from exposure to intense light.

In terms of light absorption, the retina can be reduced to two relevant layers, namely RPE and choroid. They both contain melanosomes, the primary retinal absorber in the wavelength range from approximately 300 to 1200 nm. Additionally, there are many other relatively minor absorbers: oxyhemoglobin and melanocytes in the choroid, lipofuscin and derivatives in the RPE, carotenoids (yellow pigments) in Henle's fiber layer (Borland et al. 1992), and rhodopsin contained in the photoreceptors (Figure 15.5).

In the RPE (a single-cell layer), the melanosomes—approximately 1  $\mu\text{m}$  large spheroids—are densely packed in the apical half of the cuboidal cells. Locally, the spacing between granules varies between 0 and 2  $\mu\text{m}$ . Since we are investigating thermally induced damage, the exposure duration of interest starts in the order of 10–50  $\mu\text{s}$  (concerning shorter pulses, the mechanism of damage is microbubble formation; Lee and Alt 2007; Schüle et al. 2005). As a consequence, local variations shorter than the thermal diffusion length can be neglected. Assuming that the surrounding medium has thermal properties similar to water, the diffusion length already reaches 2.5  $\mu\text{m}$  at 10  $\mu\text{s}$ . It is therefore justified to consider bulk absorption in the apical portion of the RPE, which moreover simplifies both the treatment of light distribution and solving of the heat equation (see further discussion in Section 15.7.1).

The measurement of absorption properties in solutions of extracted melanosomes is very sensitive to the experimental approach (Stolarski et al. 2002) and it cannot be directly applied to the RPE since the concentration *in situ* is not identical. Furthermore, data over the whole spectral range of interest are—to the knowledge of the authors—not available. The optical density of the RPE as a whole has been measured *in vitro* for the wavelength range of 400–1100 nm (Gabel et al. 1976), 1200 nm (Coogan et al. 1974), and 1500 nm (Geeraets et al. 1962). The data from Gabel are commonly used in a mathematical description of RPE bulk absorption. A fitting equation was first proposed by Jacques et al. (1996).

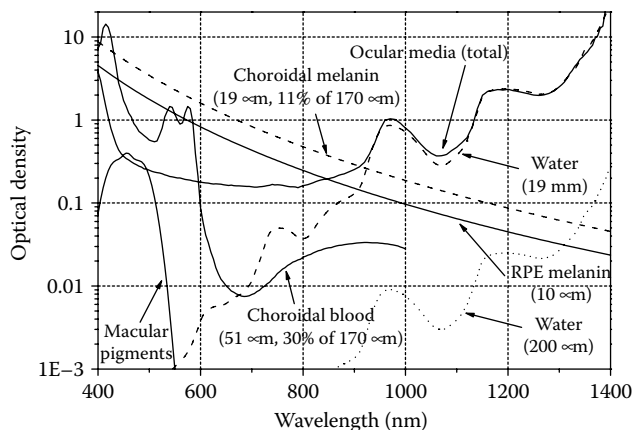


**FIGURE 15.5**

Optical density of various ocular absorbers. (Thicknesses taken from Jean, M. and Schulmeister, K., Validation of a computer model to predict laser-induced thermal injury thresholds to the retina. In: *ILSC 2013 Conference Proceedings*, Laser Institute of America 1002:229–238, 2013.)

Similar expressions in exponential or power functions are found in Vincelette et al. (2008) and Jean and Schulmeister (2013).

In the choroid, the distribution of melanosomes is much sparser as well as inhomogeneous (i.e., there is significant clustering). However, again, the assumption of a homogeneous distribution can be argued to be valid for pulse durations that are relevant for thermal injury. Indeed, since damage is mainly located at the RPE level (see Section 15.8), local variations of several tenths of micrometers in the choroid do not affect temperature diffusion as seen from the RPE. It is, however, critical to define both an appropriate equivalent layer thickness and its separation distance to the RPE, considering the observation that the outer choroid can appear under the light microscope more than two times darker than its inner part (Weiter et al. 1986).

The choroid is densely perfused by vessels of various sizes and bordered by a dense network of capillaries (Spraul et al. 1996) in which blood is highly oxygenated (~95%, commonly assimilated to pure oxyhemoglobin; Berendschot et al. 2003). With a concentration of 30%–50% in blood (e.g., Hammer et al. 1995), the red pigment found in red blood cells is a relevant absorber for wavelengths shorter than approximately 590 nm (Figure 15.5). Similarly to melanin, heterogeneous blood distribution is not critical and the choriocapillaris can also be modeled as a homogeneous blood layer with a representative absorption coefficient.

In the central region of the retina (Hammond et al. 1997), Henle's fiber layer (see Figure 15.4) possesses distinctive pigments that selectively absorb blue light (thus called yellow pigment). They are carotenoids such as xanthophylls and zeaxanthins whose function is to shield the photoreceptors from phototoxicity (Snodderly et al. 1991) induced by high-energy photons (sometimes referred to as actinic radiation). A formula in the form of exponential functions has been derived by Zagers and van Norren (2004) for their absorption spectrum (Figure 15.5).

### 15.6.1.1 Distribution of Absorbers and Layer Geometry

As seen previously, the various layers are heterogeneously pigmented from an anatomical point of view, but they can be treated in the thermal regime as equivalent homogeneously pigmented layers. Therefore, the thicknesses of the layers in a model may not be representative of the anatomical ones. Birngruber et al. (1985) have used three layers—RPE, an intermediate nonpigmented layer, and a pigmented choroid—whose thicknesses are, respectively, 5, 25, and 80  $\mu\text{m}$ ; Vogel and Birngruber (1992) have used 6, 4, and 400  $\mu\text{m}$ , while Jean and Schulmeister (2013) have chosen 10, 4, and 170  $\mu\text{m}$ , respectively. The RPE cell height is expected to lie between 10 and 12  $\mu\text{m}$  (Gabel et al. 1976; Coogan et al. 1974), depending on sources, references of measurement, and location in the retinal map. It is the thickest at the foveola and decreases with eccentricity. Choroidal thickness is often reported to be between 80 and 170  $\mu\text{m}$  (Birngruber et al. 1985; Coogan et al. 1974) following *in vitro* measurements. It has to be emphasized that *in vivo* measurements can yield up to a twofold thicker tissue, since large vessels usually collapse during manipulation (Delori and Pflibsen 1989; Birngruber 1991). Choroidal thickness, correlated with size and density of vessels, is observed to be thinner in the paramacula than in the macula of elderly human subjects (Spraul et al. 1996) but there is no evidence of any significant change over the region of interest for laser-induced damage studies in young monkey subjects (typically the central 30°).

Between the pigmented layers, the pigment-free volume consists of the basal part of RPE cells (~3–5  $\mu\text{m}$ ) and Bruch's membrane (3  $\mu\text{m}$  in elderly human subjects; Spraul

et al. 1996), and the innermost layer of the choroid is sometimes also included (about 20  $\mu\text{m}$ , Birngruber et al. 1985). Such a separation distance between the RPE and pigmented choroid has an effect of several tenths of a microsecond in delaying the heat wave traveling from the choroid toward the RPE (the RPE is the critical layer for thermal injury at threshold level). Therefore, it has a minor effect, only impacting very short pulses or exposures at the long wavelength end of IR-A where the choroid plays an important role.

### 15.6.1.2 Regional Variations

Also of importance is the variation of morphology throughout the retinal surface. Photoreceptor distribution, vessel density, layer thickness, cell dimensions, and pigment concentration are more or less concentric functions centered about the foveal pit. Concentric regions of importance in laser-induced damage experiments are marked in Figure 15.4.

The RPE cell diameter increases with distance from the foveola: the diameter reaches 13.5  $\mu\text{m}$  on average at the foveola and 18  $\mu\text{m}$  at 2–4 mm from the center (Snodderly et al. 2002). It follows that RPE cell density is twice as large in the foveal region as in the outer regions of the retina. Even if the melanosome concentration (per cell) is slightly lower in the macula than in the peripheral region (Feeney-Burns et al. 1984), pigment concentration per surface area, and consequently local optical density, is higher within the central portion (Weiter et al. 1986). Since RPE melanin also plays a role in protecting the retina from oxidative stress (Sarna 1992; Wang et al. 2006), this change in pigment concentration is consistent with the increased density of photoreceptors and subsequent metabolic activity in the central retina (Wikler and Rakic 1990). In the same fashion, fluorescence, which is correlated with the amount of RPE melanin and its derivatives, reveals a Gaussian-shaped distribution almost centered about the fovea in human subjects (Keilhauer and Delori 2006). Finally, RPE light transmission measurement allows quantification of this variation: the central region absorbs about 75% more energy than the paramacula (at approximately 3 mm away from the foveola; Gabel et al. 1978). These variations are large enough to necessitate differentiating model parameters for central or peripheral exposures. Threshold lesions require between 25% and 100% more energy in the paramacula than in the macula (for instance, see Cain et al. 2000; Lappin 1971). Variable regional sensitivities can be simulated by modifying pigment concentration or layer thickness. In the latter approach, the difference vanishes if diffusion is negligible or if the absorption depth is shorter than the layer thickness, that is, short pulse duration and short wavelength, respectively.

### 15.6.1.3 Fundus Reflectance

Due to the presence of scatterers and layers of varying refractive indices, diffuse and specular reflections occur in the retina. Backscattered light from the back of the eye (fundus) is used to examine the retina noninvasively. Since the spectral distribution of reflected light depends on the optical density of the various retinal layers, it can also be used to infer retinal pigmentation quantitatively (see review by Berendschot et al. 2003).

The sclera is a strong reflector (Delori and Pflibsen 1989), as light is both backscattered by collagen fibrils and reflected at its surface because of its relatively high refractive index (Fine et al. 1985). Other important sources of reflection are identified at the RPE level, at the inner limiting membrane as well as in the choroid (Berendschot et al.

2003). Additionally, blood, photoreceptors, and macular pigments play a substantial role in interpreting reflectance in the visible spectrum (Hammer and Schweitzer 2002). Melanin concentration, in both the RPE and the choroid, is the predominant signature of reflectance from about 600 nm to the end of the IR-A range (Hammer and Schweitzer 2002), which can reach up to 15% in lightly pigmented human individuals (Delori and Pflibsen 1989).

Quantitatively, the main part of the reflectance can therefore be approximated with a basic model consisting of two reflectors on both sides of the pigmented region. This model uses a wavelength-dependent reflection at the sclera and an eccentricity-dependent reflectance at the RPE (proposed by van Norren and Tiemeijer 1986). This basic model is satisfactory for approximating the amount of light measured out of the eye but suffers from strong simplifications such as the absence of diffusion, thus leading to an overestimation of the pigmentation (Delori and Pflibsen 1989).

A similar model has already been used in combination with a thermal model for controlling the size of photocoagulation (Pflibsen et al. 1989). It appears that the change in choroidal pigmentation is the main factor for suprathreshold lesion size variation. Therefore, reliable fundus reflectance data can effectively provide additional information on both absolute and relative pigmentation. Other approaches for the modeling of light propagation in attenuating media are discussed in Welch and van Gemert (1995).

### 15.6.2 Cornea

The cornea is the outermost transparent part of the eye, with a diameter of about 11 mm in humans. The space between the cornea and the lens of the eye is filled with the aqueous humor. The cornea acts as the primary diffractive element of the eye, while the lens serves mostly for accommodation.

In nonhuman primates from the genus *Macaca*, the central cornea is in the order of 500–550  $\mu\text{m}$  thick (Boettner and Dankovic 1974 and Maher 1978, respectively), while corneal thickness is only 300  $\mu\text{m}$  in common rabbits (Zhang et al., 2009). In general, corneal thickness is also subject to variation of ocular pressure, thickening with increasing eccentricity and interindividual variability.

Due to the high water content of the cornea (80%) and of the aqueous humor (99%), optical radiation of wavelengths longer than approximately 1.2  $\mu\text{m}$  is predominantly absorbed by these anterior media, reaching the retina or even the lens only weakly. Above a wavelength of 2.5  $\mu\text{m}$ , absorption of optical radiation is entirely concentrated in the first few hundreds of micrometers (Figure 15.6). Noticeably, for an absorption coefficient larger than 1000  $\text{cm}^{-1}$ , the penetration depth—shorter than 10  $\mu\text{m}$ —is even reduced to the tear film.

The estimation of normal tear film thickness is subject to controversy, with values ranging between 3 and 40  $\mu\text{m}$  (King-Smith et al. 2000). Differences between species are large as well (Prydal and Campbell 1992) and, depending on the environment and the application of saline (or lack thereof), evaporation plays a critical role in the evolution of the precorneal tear film thickness in the time course of minutes (Iwata et al. 1969). Thus, the method used for preventing corneal dryness during *in vivo* corneal exposures must be considered for the sake of consistency when comparing corneal lesions (Fine et al. 1968).

Scattering and refraction in the cornea are negligible for modeling corneal injury, since we are only interested in light distribution within the cornea, not behind it. It is commonly accepted that the cornea is homogeneously absorbent because it does not contain pigments and its water content is homogeneous throughout the various sublayers.

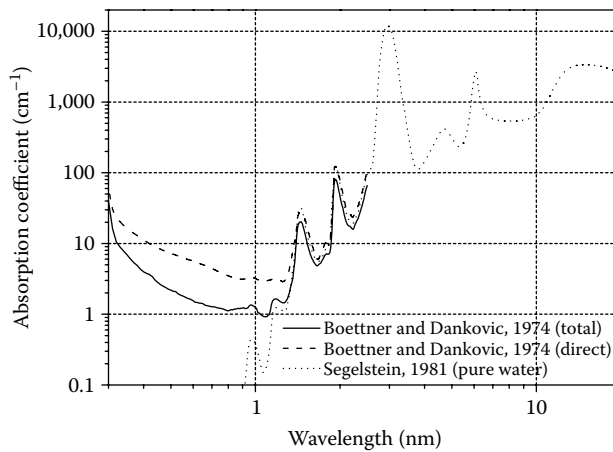


**FIGURE 15.6**  
Absorption coefficient of the rhesus monkey cornea (sampled up to 2.5  $\mu\text{m}$ ) and of pure water.

The Beer–Lambert law, which describes the exponential decay of local irradiance with distance, is used to calculate optical attenuation within the cornea (thus referring to absorption coefficient). Specular reflection at the front surface can be taken into account by the Fresnel equations. The assumption that the corneal refractive index is similar to that of water for all wavelengths of relevance is thought to be acceptable (e.g., data from Segelstein 1981). At the interface between cornea and aqueous, reflection (corresponding to the second Purkinje image) is assumed to be negligible given the small difference between refractive indices.

From a thermal point of view, we believe that the curvature of the cornea does not play a substantial role for modeling. Simple geometrical optics allows confirmation that optical power does not constitute a primary variable. By applying Snell’s law of refraction, it can be shown that the largest angle of refraction reaches only  $11^\circ$  (worst case obtained with a centered and collimated 8 mm beam). The larger the beam, the less important local variations at the edges become. Thus it can be assumed that the beam diameter remains constant throughout the corneal depth, unless the laser beam is strongly focused to a tiny spot at the corneal surface.

## 15.7 Heat Transfer

### 15.7.1 Heat Equation

When addressing the issue of thermal interaction in the modeling of laser-induced thermal injury at threshold level, only heat generation and conduction are critical. Convection and evaporation are secondary, while metabolism—through the rate of work performed continuously within the tissue—and radiation from the cornea are comparatively negligible (Chen et al. 2006; McCally et al. 1992). Consideration of vascular convection in the case of the retina and free air convection on the corneal surface

are discussed below. In this context, the distribution of heat over space and time is described by the heat equation of conduction including a source term resulting from the absorption of laser radiation. In its differential form and in cylindrical coordinates, this is written as:

$$\frac{\partial T(r, \theta, z, t)}{\partial t} - \alpha \Delta T(r, \theta, z, t) = q_s(r, \theta, z, t)$$

where:

$T$  is the increase in temperature (K)

$\alpha$  is the thermal diffusivity ( $\text{m}^2 \text{s}^{-1}$ )

$q_s$  is the source term ( $\text{W m}^{-3}$ )

As the laser beam and the local tissue usually feature axial symmetry, the angular component  $\theta$  vanishes and the problem can be reduced to two dimensions ( $r$  for radius and  $z$  for depth). The symmetry is lost in cases of complex beam profiles and scanning.

The equation is linear with respect to laser power, provided that thermal properties are constant (i.e., are assumed not to depend on temperature). Variation in thermal diffusivity of water does not exceed 7% between 40°C and 80°C, thus having a very limited impact on damage levels. Within the retina, melanosomes exhibit a significantly higher mass density ( $\sim 1400 \text{ kg m}^{-3}$ ) and lower specific heat capacity ( $\sim 2700 \text{ J kg}^{-1} \text{ K}^{-1}$ ) than water (Neumann et al. 2005). Nevertheless, only the product of these two properties is relevant and it remains similar to that of water. This approximation is convenient since it greatly simplifies the problem geometry and the solving process. In general, biological tissues are 10%–20% less thermally conductive than water (e.g.,  $0.58 \text{ W m}^{-1} \text{ K}^{-1}$  in Ooi et al. 2008; nonlinear relation as a function of water content in Chen et al. 2006). In addition to conduction, heat convection can take place in vascular layers (e.g., choroid) or on both sides of the cornea (due to temperature gradient at the air/cornea interface and aqueous flow; Ooi and Ng 2008). A convenient approach is to consider convection as simple heat dissipation or, in other words, as removal of heat from the system. The concept of heat sink represents losses without transfer from one location to another and is mathematically formulated in the heat equation as an additional and negative source term on its right-hand side (see derivation in Roeder and Birngruber 1995):

$$q_b(T) = \rho_b c_b w_b (T_b - T)$$

where the terms on the right-hand side are, from left to right, mass density, specific heat capacity, perfusion rate, and incoming blood temperature (SI units). The perfusion rate is expressed in  $\text{sec}^{-1}$  (e.g.,  $1 \text{ sec}^{-1}$  means 100% of the perfused tissue is renewed within 1 sec by tissue at body temperature). Perfusion rates in the range of  $0.15\text{--}0.35 \text{ sec}^{-1}$  have been estimated in the rabbit retina (Kandulla et al. 2006; Herrmann et al. 2007). The assumption of global perfusion underestimates real flow rates but at the same time it overestimates heat losses since heat vanishes instead of being actually displaced. In general, modeling of blood flow is relevant only for exposure durations longer than several seconds (Welch et al. 1980; Birngruber et al. 1985). A different approach for heat convection is addressed in the next section.

### 15.7.2 Initial and Boundary Conditions

In association with the heat equation, it is necessary to define initial and boundary conditions. Initially, the temperature distribution is at equilibrium—that is, body temperature—and constant throughout the retina:

$$T(t = 0) = T_{\text{body}}$$

In the case of tissues at the body surface, three approaches are discussed. First, a constant temperature can be assumed because, as the temperature gradient is close to  $0.3 \text{ K mm}^{-1}$  (Ng and Ooi 2007), the much larger local temperature increase required to induce damage makes such variation secondary.

This can, however, be refined by imposing heat transfer at the corneal surface. Scott (1988a) proposed a model and numerical values for taking into account evaporation, free air convection, and radiation:

$$-k \cdot \frac{\partial T(z=0)}{\partial z} = q_e + h(T - T_\infty) + \sigma \epsilon (T^4 - T_\infty^4)$$

In the field of laser-induced damage, this boundary model—neglecting emissivity—has been applied to the skin by Chen et al. (2006). It includes a temperature-dependent outward flux for modeling vaporization. It is expected to underestimate heat loss at the corneal surface since—although lipid components slow down evaporation—the tear film remains subject to loss of water to a greater extent than the comparatively drier epidermis.

In normal conditions, say at an ambient temperature of  $22^\circ\text{C}$ , evaporation accounts for  $40\text{--}100 \text{ W m}^{-2}$ , free convection for  $120 \text{ W m}^{-2}$ , and radiation for  $30 \text{ W m}^{-2}$  (data from Scott 1988a). The steady-state temperature can be obtained by solving the time-independent heat equation or it can be approximated by a linear equation (the gradient being approximately  $0.38 \text{ K mm}^{-1}$  in Scott's data):

$$T(t = 0) = T_{\text{surface}} + z \cdot \frac{dT}{dz}$$

Alternatively, when using numerical methods, it is possible to take into account a volume of air in front of the cornea, in which case outward conduction and convection can be included directly in the heat equation. Calculations by the authors show that the two approaches give almost identical results (within 10% for typical spot sizes and absorption coefficients). Explanations for this similitude are (i) the investigated pulse durations are too short for observing a significant difference, (ii) the differences are insignificant regarding the relatively large temperature increase within the cornea, and (iii) the model and values proposed by Chen et al. (2006) for the skin may underestimate heat losses at the cornea.

Due to the transient nature and the extent of the temperature rise, parameterizing the boundary conditions does not impact threshold levels much. It follows that the initial surface temperature is actually of greater importance than the aforementioned assumptions on boundary conditions. The normal corneal surface temperature fluctuates by about  $1^\circ\text{C}$  around  $34^\circ\text{C}$  (e.g., Mapstone 1968; Scott 1988a) depending on several factors such as ambient temperature, humidity, circadian phase, anesthesia, and blink rate.

Using numerical methods, boundary conditions are usually of the Neumann type due to the limited volume being modeled. That is, the normal component of the temperature derivative is set to zero. In a two-dimensional problem with axial symmetry, it writes:

$$\vec{r} \cdot \frac{\partial T(r, \vartheta, z, t)}{\partial r} \Big|_{r=0, r=R} = \vec{z} \cdot \frac{\partial T(r, \vartheta, z, t)}{\partial z} \Big|_{z=0, z=Z} = 0$$

### 15.7.3 Solving the Bioheat Equation

Under certain circumstances (symmetry, homogeneity, etc.), analytical solutions of the bioheat equation can be found. A review of the solutions in the field of laser–tissue interactions was published by Roider and Birngruber (1995). Noticeably, a semianalytical solution to the specific problem of laser-heated retina using a Gaussian laser beam profile and exponentially decaying absorption has been developed by Birngruber et al. (1978) but its formulation in the form of error functions impedes numerical evaluation for high levels of absorption (e.g., those relevant in the short-wavelength range). An unconditional stable analytical solution exists, however, for a sphere. Its application to the problem of retinal laser irradiation consists of considering each melanin granule as a spherical absorber embedded in an infinite homogeneous medium. The linearity of temperature with respect to laser power makes it possible to superimpose the solutions obtained for a set of spheres (typically a few thousand) at any time and at any location in space. The approach developed by Thompson et al. (1996) (referred to as the Thompson Gerstman model) takes intergranule shading into account and serves as a valuable basis for modeling short-term variations in temperature at the micrometer scale, that is, within and between melanosomes. Phenomena relevant to short pulse exposures are mainly hot spots and microbubble formation. A drawback is that this approach is inherently associated with homogeneous properties and infinite volumes. Consequently, significant limitations of analytical solutions and today’s powerful computational methods give growing support for the use of numerical solutions. They simplify the treatment of nonlinearity, allow for the introduction of inhomogeneities and handling of complex geometries. These potentials, although still not fully capitalized in current models, may prove beneficial in the future.

Among numerical methods, the finite element method (FEM) appears to be the most enticing, as user-friendly and powerful commercial software is available. As with other methods, such as finite differences, the fundamental concept relies on discretization. The mathematical and computational procedures are beyond the scope of this chapter but they are widely discussed in the literature (e.g., Reddy and Gartling 2001). The FEM has already been applied for the modeling of ocular temperature (Ng and Ooi 2007), ocular hyperthermia, (e.g., Scott 1988b) and retinal coagulation (Glenn et al. 1996).

### 15.7.4 Characteristic Results

In this section, absolute threshold levels are not discussed because they depend on various model parameters, the type of tissue studied, the species involved, and so on, but it is worth highlighting the fundamental characteristics shared by all models. Retinal and corneal models typically exhibit the same trends when results are observed as a function of exposure duration, spot size, or absorption coefficient (i.e., wavelength).

As the damage mechanism is purely thermal, three regimes can be distinguished: (i) thermal confinement, where heat diffusion does not apply, (ii) transient phase where heat diffusion is under progress, and (iii) steady state where conduction of heat away from the source has reached equilibrium.

Two interesting asymptotic behaviors are mathematically described by the definition of internal energy and Fourier's law, respectively:

$$\left\{ \begin{array}{l} \text{thermal confinement: } \frac{\Delta T}{Q} = \frac{1}{\rho c V} \\ \text{steady state: } \frac{\Delta T}{Q} = \frac{l}{S \kappa t} \end{array} \right.$$

where:

$Q$  is the absorbed energy

$\Delta T$  is the increase in temperature

$\rho$  is the mass density

$c$  is the specific heat capacity

$V$  is the volume

$S$  is the surface of conduction

$\kappa$  is the conductivity

$t$  is the time

$l$  is a characteristic length (all in SI units)

Regarding the spatial variables, one can consider an idealized heated volume that is radially delineated by the spot radius and by the penetration depth in the depth dimension, conceptually representative of a thin cylinder, whose total surface area is assumed to be representative of the exchange surface of conduction. Finally, the characteristic length is set to the spot radius since it has been shown to be a good measure of thermal diffusion (Schulmeister et al. 2006).

These basic regimes are compared with model simulations in Figure 15.7a (run with arbitrary parameters; typical for the macula at 530 nm). The ordinate (in kelvin per joule) is representative of the heat capacity of the system. Besides the fact that the two aforementioned limiting cases are time independent and inversely proportional to time, respectively, we observe a breakpoint whose position varies with spot size in a following a power law with respect to time (Figure 15.7b). This relationship becomes inexact for very small spots because the definitions of volume and surface are inappropriate.

The theoretical breakpoint can be simply calculated by resolving the system of equations mentioned before. It is worth mentioning that damage thresholds (expressed as energy) do not exactly vary linearly with respect to time in the long exposure regime because the damage model is nonlinear (purposely neglected in this study in order to characterize the purely thermal behavior of the laser/tissue system).

A similar analysis of the thermal interaction in our laser/tissue system can be performed over the dependence of thresholds on spot size. Three regimes are clearly identified (see Schulmeister et al. 2006): (1) a constant threshold level below a certain spot size, referred to as minimum angular subtense, (2) a variation proportional to the square of the spot size (i.e., to the surface area) above a certain spot size, referred to as maximum angular subtense, and (3) a transition phase that can be approximated (for instance in laser safety guidelines) to vary linearly with spot size.

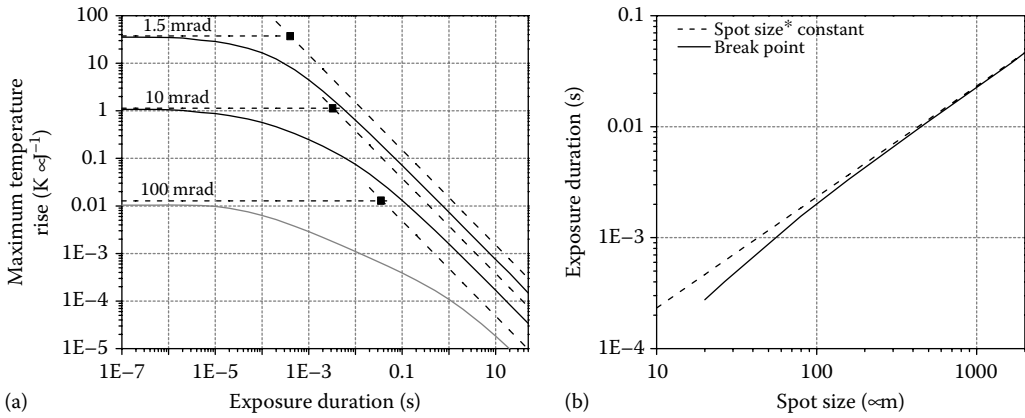


**FIGURE 15.7** (a) Representation of the thermal capacity of the retina by asymptotic analysis. (b) Variation of the breakpoint in time with retinal spot size.

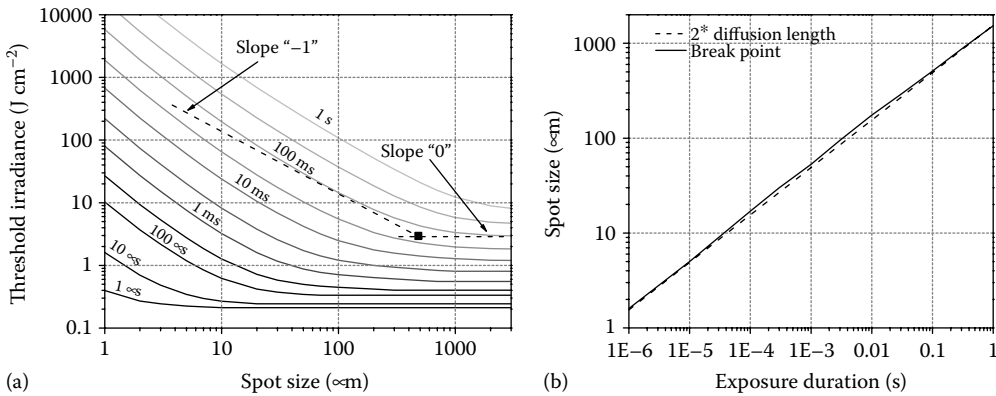


**FIGURE 15.8** Threshold irradiance as function of spot size for various exposure durations; at each exposure duration, the cross-point between asymptotes representative of slope 0 and -1 yields a spot size, which can be directly compared with twice the diffusion length.

When irradiance thresholds are plotted as a function of spot size, a breakpoint is also identified by examining the asymptotic behavior (Figure 15.8a). For each exposure duration, this breakpoint is compared with the theoretical diffusion length that applies to this duration (Figure 15.8b). A good agreement is therefore indicative of a direct correlation between the spot size and the effect of radial diffusion with respect to time.

## 15.8 Modeling of Damage

### 15.8.1 Lesion Definition

The definition of a lesion is dependent on the observation method and the scale as well as the investigated tissue reaction (referred to as end point). For safety reasons, a threshold

injury is roughly defined as the smallest lesion that can be reasonably detected with a given method, usually under ophthalmoscopic examination. In laser safety, what is referred to as “threshold” is the statistical product of results from several exposures at various energy levels (doses), and it represents the dose at which 50% of exposures lead to an observable injury (known as ED<sub>50</sub>; its relevancy is discussed in Sliney et al. 2002). This experimentally determined value is commonly taken as a reference for the validation of a threshold injury computer model.

The damage mechanism discussed here is purely thermal in nature. At the subcellular level and at threshold level, elevated temperatures lead to denaturation of proteins, which leads to cascading processes that ultimately kill the cell if a sufficient fraction of critical proteins have been affected. Proteins are plausible targets as they are basic cellular components. Proteins can undergo unfolding—a potentially reversible process—above melting temperature. This transition occurs above 42°C–47°C (Deaton et al. 1990; Lepock 2003; Dewirsh et al. 2003). Accumulation of denatured proteins within a cell impedes vital functions and if repair mechanisms are insufficient, the cell ultimately dies. Several observations tend to confirm that a single mechanism, namely protein denaturation, is the basis of thermally induced injuries across a wide variety of tissues and over a wide range of temperatures (Lepock 2003). In the case of retinal damage, preferred targets might be the melanosome coat or cellular membranes (Wright 2003). At the cellular level, thermally induced injury is associated with cell death. A severe insult involves necrosis, characterized by swelling followed by removal of cell debris through phagocytosis (Verheyen 1996). Histopathological studies suggest that this process is dominant following intense increase in temperature (i.e., short exposure, Zuclich et al. 1998; Marshall et al. 1975). Apoptosis occurs mostly after moderate thermal insult and this process lasts longer (Matylevitch et al. 1998) since the cell can be only partially damaged without its integrity being compromised, that is, the cell can still fight to recover homeostasis (Verheyen 1996). This may explain the observation of increasing delay in the appearance of threshold lesions following long exposures (i.e., up to 48 h after second-long exposures).

When the temperature rise exceeds approximately 20°C for a very short period, there is strong evidence that thermotolerance does not play any role during the heating time (Dewirsh et al. 2003), although the synthesis of protective products (heat shock proteins) is already triggered (Desmettre et al. 2001). The effect of long exposures involving relatively low temperature increases (i.e., 10–15°C) may however be impacted by thermotolerance at threshold level (Deaton et al. 1990). A schematic representation in Figure 15.9 gives a simplified review of the damaging process.

### 15.8.2 Mathematical Description

The effect of temperature on organic components has been widely studied in biochemistry and the rate of chemical reactions can be described mathematically by the Arrhenius equations. In the so-called Arrhenius model, a rise in temperature defines the rate at which a given reaction occurs, assuming that the pathway remains identical. The temperature-dependent reaction rate is given by:

$$k(t) = A \cdot e^{\frac{-E}{T(t)}}$$

where:

$T$  is the absolute temperature (K)

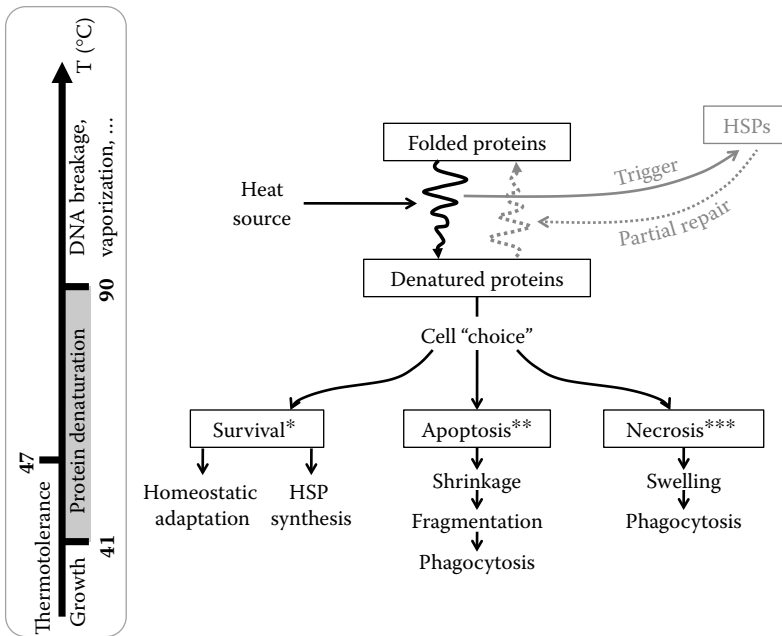


**FIGURE 15.9** Schematic of simplified processes and scenarios of cellular response to acute heat stress (responses to \* light, \*\* moderate, and \*\*\* severe heating).

$A$  is a frequency factor ( $\text{sec}^{-1}$ )

$E$  is an inactivation energy divided by the gas constant (K)

The factor  $A$  is assumed to be temperature independent (Jacques 2006; Criado 2005; a temperature-dependent formulation is provided by the Eyring equation). Subdamage accumulation  $\Omega$  is then described by its integration over time, which leads to:

$$\Omega = \int_0^t k(t) dt$$

This measure of damage also has a statistical interpretation. The cell or tissue is conceived as a system containing billions of targets that are, independently from each other, transformed to a degenerative state of lower energy (e.g., protein unfolding). A macroscopic observation of this phenomenon leads to an overall single process, represented by a concentration of affected targets:

$$C_{\text{denaturated}} = 1 - e^{-\Omega}$$

Setting  $\Omega = 1$  corresponds therefore to 63% of damaged targets (commonly accepted for representing threshold damage). It has also been suggested that 5% is enough to achieve cell death (Lepock 2003) but these numerical values and their importance must be put into perspective because they are directly dependent on the choice of the preexponential factor.

For instance, different degrees of skin burns (redness, edema, thrombosis) can be modeled with a single set of Arrhenius parameters simply by associating the different degrees of lesion with appropriate values of  $\Omega$  (Henriques 1947).

It appears that this first-order model is appropriate in the range of time and temperatures under investigation. It is worth mentioning that the timescale at which protein dynamics occurs is much shorter than the laser exposure in the thermal regime (Day et al. 2002). It follows that the dynamics of each molecular reaction can be neglected. Furthermore, we are only interested in quantifying the first step of the cellular damage process or, in other words, only the component that is the most sensitive to a temperature rise (known as the limiting step). Subsequent reactions are triggered in cascade. In the case of very long exposures (several minutes to hours), a model of higher order might be necessary (Jacques 2006) since long-term processes such as thermotolerance or refolding come into play and can partly counterbalance the destructive action of temperature increase.

As shown by Wright (2003) and Jacques (2006), the two coefficients of the Arrhenius integral can be mathematically linked (see Gibbs free energy and Van't Hoff equation) so that only one independent coefficient is representative of the chosen end point. The inactivation energy commonly used for cutaneous, corneal, and retinal injuries is consistent with the order of magnitude characteristic of protein denaturation (100–200 kcal mol<sup>-1</sup> or 50,000–100,000 K; Deaton et al. 1990; Lepock 2003). It has been inferred that all corneal layers—epithelium, stroma, and endothelium—have similar sensitivity to elevated temperature, thus allowing the use of a unique set of damage parameters for the whole tissue (Farrell et al. 1985). Some values found in the literature are plotted in Figure 15.10a. These curves show the temperature jump required for achieving an isoeffect (in this case for modeling minimum injury). The approximate intersection—suggestive of a typical transition temperature—is believed to be representative of the general form of thermal damage. The discrepancies between sets of parameters may not be of physical meaning but, instead, may be attributed to possible inconsistencies between end points, possible inconsistencies between model parameters, or the fact that the various models have not been validated against the same set of experimental results.

To our knowledge, there are few alternatives to the Arrhenius approach. An empirical time-dependent critical temperature has been applied to both minimal damage

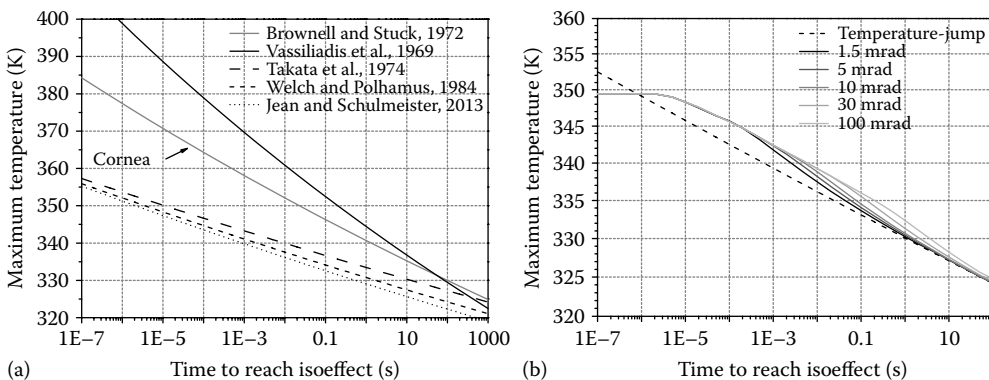


**FIGURE 15.10**

(a) Isoeffect curves for various Arrhenius sets applied in models of retinal and corneal damage. (b) Comparison between temperature-jump assumption and simulated time-temperature histories.

and vaporization (Barger et al. 1989) but doubt remains regarding its applicability to exposures shorter than about 10 ms (McCally et al. 1992).

### 15.8.3 Lesion Size and Computation

The Arrhenius model must be solved iteratively (e.g., up–down method) by scaling the increase in temperature in order to find the unique exposure level that leads to  $\Omega = 1$ . One can take advantage of the linearity of the heat equation with regards to power by solving it once for an arbitrary exposure level and subsequently scaling the temperature to reach threshold. When computation time is of importance, this is a reason for assuming model properties that retain linearity (such as constant and homogeneous thermal properties).

Several investigators have examined the size of ophthalmoscopic minimum visible lesions (MVL) by means of histological sections or flat preparations (e.g., Welch and Polhamus 1984; Bresnick et al. 1970). It appears that thermally induced lesions are detectable down to a size of 30–50  $\mu\text{m}$  although variability increases under approximately 80  $\mu\text{m}$  (Vincelette et al. 2008). It is known that the MVL is at least as large as one epithelial cell in *in vitro* conditions, that is, 10–20  $\mu\text{m}$  in diameter (Milsom et al. 2006). The assessment of an MVL is also impacted by several parameters not related to its actual size: optical quality, contrast and dynamic range of the ophthalmoscopic apparatus, delay after exposure, damage depth (i.e., wavelength), pigmentation, local molting, and changes in contrast over the retinal map, among others. In the cornea, lesions investigated with a slit lamp are detectable between 80  $\mu\text{m}$  (Stuck et al. 1981) and 200  $\mu\text{m}$  (Byer et al. 1972).

Since MVL are finite in size, damage must be numerically evaluated also over a certain tissue volume. Given the fact that the beam profile for threshold experiments is either top hat or Gaussian and exhibits axial symmetry, it follows that the temperature will always decrease monotonically with increasing distance from the spot center. As a consequence, if damage is detected at a distance  $r_0$ , the domain that satisfies  $r \leq r_0$  is *de facto* damaged. The increase in temperature must be monitored at the edge of the MVL domain only. Most thermal models have been developed with MVL diameter between 20 and 50  $\mu\text{m}$  (Takata et al. 1974; Birngruber et al. 1985).

Within the tissue of interest, the depth where the model calculates the damage integral can be set as an input parameter or alternatively the lesion depth can be detected automatically as the depth at which the increase in temperature is maximum. According to histological findings, retinal lesion is located at the RPE level, where absorption density is the highest. Histopathological studies confirm the good agreement found between cellular effects and ophthalmoscopic observations (Zuclich et al. 1998; Marshall et al. 1975). In modeling, it has always been implicitly assumed that the MVL thickness is infinitesimal.

The Arrhenius parameters can be obtained experimentally from temperature measurements during typical threshold exposures. Plotted as a function of exposure duration, one can determine the most appropriate model coefficients (see experimental data by Moritz and Henriques 1947; Welch and Polhamus 1984). Nevertheless, this method requires the assumption of an instantaneous steady-state temperature (referred to as temperature jump) during the entire exposure. This is, however, not correct in the microsecond and millisecond regime and it introduces a bias. A simulation run with typical time–temperature histories for retinal damage calculated by the authors shows the extent of this error (Figure 15.10b). In view of this discrepancy and the fact that temperature measurements

often suffer from significant errors (response delay in the microsecond regime, superficial measurement, and probe positioning), the discrepancies observed in Figure 15.10a are easily put into perspective.

---

## References

- Atchison, D.A. and G. Smith. 2000. *Optics of the Human Eye*. Edinburgh: Butterworth-Heinemann.
- Atchison, D.A. and G. Smith. 2005. Chromatic dispersions of the ocular media of human eyes. *J Opt Soc Am A* 22(1):29–37.
- Bargerion, C.B., O.J. Deters, R.A. Farrell and R.L. McCally. 1989. Epithelial damage in rabbit corneas exposed to CO<sub>2</sub> laser radiation. *Health Phys* 56(1):85–95.
- Berendschot, T.T.J.M., P.J. DeLint and D. van Norren. 2003. Fundus reflectance: Historical and present ideas. *Prog Retin Eye Res* 22:171–200.
- Birngruber, R., F. Hillenkamp and V.-P. Gabel. 1978. Experimentelle und theoretische Untersuchungen zur thermischen Schädigung des Augenhintergrundes durch Laserstrahlung. Report AO 251. Munich: Gesellschaft für Strahlen- und Umweltforschung (German).
- Birngruber, R., E. Drechsel, F. Hillenkamp and V.-P. Gabel. 1979. Minimal spot size on the retina formed by the optical system of the eye. *Int Ophthalmol* 1(3):175–178.
- Birngruber, R., V.-P. Gabel and F. Hillenkamp. 1983. Experimental studies of laser thermal retinal injury. *Health Phys* 44(5):519–531.
- Birngruber, R., F. Hillenkamp and V.-P. Gabel. 1985. Theoretical investigations of laser thermal retinal injury. *Health Phys* 48(6):781–796.
- Birngruber, R. 1991. Choroidal circulation and heat convection at the fundus of the eye. In *Laser Applications in Medicine and Biology*, ed. M.L. Wolbarsht, Vol. 5, pp. 277–361. New York: Plenum.
- Boettner, E.A. and D. Dankovic. 1974. Ocular absorption of laser radiation for calculating personnel hazards. Final report. Brooks City-Base, TX: USAF School of Aerospace Medicine.
- Borland, R.G., P.A. Smith and G.P. Owen. 1992. A model for the prediction of eye damage from pulsed lasers. *Laser Light Ophthalmol* 5(2):61–67.
- Bradley, D.V., A. Fernandes, M. Lynn, M. Tigges and R.G. Boothe. 1999. Emmetropization in the rhesus monkey (*Macaca mulatta*): Birth to young adulthood. *Invest Ophthalmol Vis Sci* 40(1):214–229.
- Bresnick, G.H., G.D. Frisch, J.O. Powell, B.M. Landers, G.C. Holst and A.G. Dallas. 1970. Ocular effects of argon laser radiation; I: Retinal damage threshold studies. *Invest Ophthalmol* 9(11):901–910.
- Buitelvelde, H., J.M. Hakvoort and M. Donze. 1994. The optical properties of pure water. In *Proceedings of SPIE, Ocean Optics XII*, ed. J.S. Jaffe, pp. 174–183.
- Byer, H.H., E. Carpino and B.E. Stuck. 1972. Determination of the thresholds of CO<sub>2</sub> laser corneal damage to Owl monkeys, Rhesus monkeys and Dutch-belted rabbits. Final report. Frankford Arsenal, PA: US Army.
- Cain, C.P., C.A. Toth, R.J. Thomas, et al. 2000. Comparison of macular versus paramacular retinal sensitivity to femtosecond laser pulses. *J Biomed Opt* 5(3):315–320.
- Chen, B., S.L. Thomsen, R.J. Thomas and A.J. Welch. 2006. Modeling thermal damage in skin from 2000-nm laser irradiation. *J Biomed Opt* 11(6):064028.
- Connolly, J.S., H.W. Hemstreet and D.E. Egbert. 1978. Ocular hazards of picosecond and repetitive-pulsed lasers. Vol. II: Argon-ion laser. Report SAM-TR-78-21. Brooks City-Base, TX: USAF School of Aerospace Medicine.
- Coogan, P.S., W.F. Hughes and J.A. Molsen. 1974. Histologic and spectrophotometric comparisons of the human and rhesus monkey retina and pigmented ocular fundus. Final report. Brooks City-Base, TX: USAF School of Aerospace Medicine.
- Criado, J.M., L.A. Pérez-Maqueda and P.E. Sánchez-Jiménez. 2005. Dependence of the preexponential factor on temperature. *J Therm Anal Calorim* 82:671–675.

- Davis, T.P. and W.J. Mautner. 1969. Helium-Neon laser effects on the eye. Report C106-59223. Fort Detrick, MD: US Army Medical Research & Development Com.
- Day, R., B.J. Bennion, S. Ham and V. Daggett. 2002. Increasing temperature accelerates protein unfolding without changing the pathway of unfolding. *J Mol Biol* 322:189-203.
- Deaton, M.A., D.G. Odom, A.M. Dahlberg, P. Lester, B.L. Cowan and D.J. Lund. 1990. Increased synthesis of heat shock proteins and partial protection of the retina against the damaging effects of argon laser irradiation. *Laser Life Sci* 3(3):177-185.
- Delori, F.C. and K.P. Pflibsen. 1989. Spectral reflectance of the human ocular fundus. *Appl Opt* 28(6):1061-1077.
- Desmettre, T., C.-A. Maurice and S. Mordon. 2001. Heat shock protein hyperexpression on chorio-retinal layers after transpupillary thermotherapy. *Invest Ophthalmol Vis Sci* 42(12):2976-2980.
- Dewhurst, M.W., B.L. Vigiante M. Lora-Michiels, M. Hanson and P.J. Hoopes. 2003. Basic principles of thermal dosimetry and thermal thresholds for tissue damage from hyperthermia. *Int J Hyperthermia* 19(3):267-294.
- Farrell, R.A., R.L. McCally, C.B. Barger and W.R. Green. 1985. Structural alterations in the cornea from exposure to infrared radiation. Technical report. Fort Detrick, MD: US Army Med Res & Dev Com.
- Feeney-Burns, L., E.S. Hilderbrand and S. Eldridge. 1984. Aging human RPE: Morphometric analysis of macular, equatorial and peripheral cells. *Invest Ophthalmol Vis Sci* 25(2):195-200.
- Fine, B.S., S. Fine, L. Feigen and D. MacKeen. 1968. Corneal injury threshold to carbon dioxide laser irradiation. *Am J Ophthalmol* 66(1):1-15.
- Fine, I., E. Loewinger, A. Weinreb and D. Weinberger. 1985. Optical properties of the sclera. *Phys Med Biol* 30(6):565-571.
- Gabel, V.-P., R. Birngruber and F. Hillenkamp. 1976. Die Lichtabsorption am Augenhintergrund. Report A 55. Munich: Gesellschaft für Strahlen- und Umweltforschung (German).
- Gabel, V.-P., R. Birngruber and F. Hillenkamp. 1978. Visible and near infrared in pigment epithelium and choroid. In: *XXIII Concilium Ophthalmologicum*, ed. K. Shimuzu and J.A. Oosterhuis, Excerpta Medica, 658:62.
- Geeraets, W.J., R.C. Williams, G. Chan, W.T. Ham, D. Guerry and F.H. Schmidt. 1962. The relative absorption of thermal energy in retina and choroid. *Invest Ophthalmol* 1(3):340-347.
- Gerrard, A. and J.M. Burch. 1994. *Introduction to Matrix Methods in Optics*. New York: Dover.
- Glenn, T.N., S. Rastegar and S.L. Jacques. 1996. Finite element analysis of temperature controlled coagulation in laser irradiated tissue. *IEEE Trans Biomed Eng* 43(1):79-87.
- Glickman, R.D. 2002. Phototoxicity to the retina: Mechanisms of damage. *Int J Toxicol* 21:473-490.
- Hammer, M., A. Roggan, D. Schweitzer and G. Müller. 1995. Optical properties of ocular fundus tissues: An *in vitro* study using the double-integrating-sphere technique and inverse Monte Carlo simulation. *Phys Med Biol* 40:963-978.
- Hammer, M. and D. Schweitzer. 2002. Quantitative reflection spectroscopy at the human fundus. *Phys Med Biol* 47:179-191.
- Hammond, B.R., B.R. Wooten and D.M. Snodderly. 1997. Individual variations in the spatial profile of human macular pigment. *J Opt Soc Am A* 14(6):1187-1196.
- Henderson, R. and K. Schulmeister. 2004. *Laser Safety*. New York: Taylor & Francis.
- Henriques, F.C. and A.R. Moritz. 1947. Studies of thermal injury. I: The conduction of heat to and through skin and the temperatures attained therein. A theoretical and an experimental investigation. *Am J Pathol* 23(4):531-549.
- Herrmann, K., C. Flöhr, J. Stalljohann, et al. 2007. Influence of choroidal perfusion on retinal temperature increase during retinal laser treatments. In *Proceedings of SPIE, Therapeutic Laser Applications and Laser-Tissue Interactions III*, ed. A. Vogel, SPIE Publishing, 6632.
- Hodgkinson, I.J., P.B. Greer and A.C.B. Molteno. 1994. Point-spread function for light scattered in the human ocular fundus. *J Opt Soc Am A* 11(2):479-486.
- Iwata, S., M.A. Lemp, F.J. Holly and C.H. Dohlman. 1969. Evaporation rate of water from the precorneal tear film and cornea in the rabbit. *Invest Ophthalmol* 8(6):613-619.
- Jacques, S.L. 2006. Ratio of entropy to enthalpy in thermal transitions in biological tissues. *J Biomed Opt* 11(4):041108.

- Jacques, S.L., R.D. Glickman and J.A. Schwartz. 1996. Internal absorption coefficient and threshold for pulsed laser disruption of melanosomes isolated from retinal pigment epithelium. In *Proceedings of SPIE, Laser-Tissue Interaction VII*, ed. S.L. Jacques, SPIE Publishing 2681:468–477.
- Jean, M. and K. Schulmeister. 2013. Validation of a computer model to predict laser induced thermal injury thresholds to the retina. In *ILSC 2013 Conf Proceedings, Laser Institute of America* 1002:229–238.
- Kandulla, J., H. Elsner, R. Birngruber and R. Brinkmann. 2006. Noninvasive optoacoustic online retinal temperature determination during continuous-wave laser irradiation. *J Biomed Opt* 11(4):041111.
- Keilhauer, C.N. and F.C. Delori. 2006. Near-infrared autofluorescence imaging of the fundus: Visualization of ocular pigment. *Invest Ophthalmol Vis Sci* 47(8):3556–3564.
- King-Smith, P.E., B.A. Fink, N. Fogt, K.K. Nichols, R.M. Hill and G.S. Wilson. 2000. The thickness of the human precorneal tear film: Evidence from reflection spectra. *Invest Ophthalmol Vis Sci* 41(11):3348–3359.
- Lappin, P.W. 1971. Assessment of ocular damage thresholds for laser radiation. *Am J Optom Arch Am Acad Optom* 48(7):600–606.
- Lee, H., C. Alt, C.M. Pitsillides and C.P. Lin. 2007. Optical detection of intracellular cavitation during selective laser targeting of the retinal pigment epithelium: Dependence of cell death mechanism on pulse duration. *J Biomed Opt* 12(6):064034.
- Lepock, J.R. 2003. Cellular effects of hyperthermia: Relevance to the minimum dose for thermal damage. *Int J Hyperthermia* 19(3):252–266.
- Lund, D.J., P.R. Edsall, B.E. Stuck and K. Schulmeister. 2007. Variation of laser-induced retinal injury thresholds with retinal irradiated area: 0.1-s duration, 514-nm exposures. *J Biomed Opt* 12(2):024023.
- Lund, D.J., P. Edsall and B.E. Stuck. 2008a. Spectral dependence of retinal thermal injury. *J Laser Appl* 20(2):76–82.
- Lund, B.J., D.J. Lund and P.R. Edsall. 2008b. Laser-induced retinal damage threshold measurements with wavefront correction. *J Biomed Opt* 13(6):064011.
- Maher, E.F. 1978. Transmission and absorption coefficients for ocular media of the rhesus monkey. Final report. Brooks City-Base, TX: USAF School of Aerospace Medicine.
- Mapstone, R. 1968. Determinants of corneal temperature. *Br J Ophthalmol* 52:729–741.
- Marshall, J., A.M. Hamilton and A.C. Bird. 1975. Histopathology of ruby and argon lesions in human and monkey retina. *Br J Ophthalmol* 59:610–629.
- Matyevitch, N.P., S.T. Schuschereba, J.R. Mata, et al. 1998. Apoptosis and accidental cell death in cultured human keratinocytes after thermal injury. *Am J Pathol* 153(2):567–577.
- McCally, R.L., R.A. Farrell and C.B. Barger. 1992. Cornea epithelial damage thresholds in rabbits exposed to Tm:YAG laser radiation at 2.02  $\mu\text{m}$ . *Laser Surg Med* 12:598–603.
- Milsom, P.K., S.J. Till and G. Rowlands. 2006. The effect of ocular aberrations on retinal laser damage thresholds in the human eye. *Health Phys* 91(1):20–28.
- Moritz, A.R. and F.C. Henriques. 1947. Studies of thermal injury. II: The relative importance of time and surface temperature in the causation of cutaneous burns. *Am J Pathol* 23(5):695–720.
- Neumann, J. and R. Brinkmann. 2005. Boiling nucleation on melanosomes and microbeads transiently heated by nanosecond and microsecond laser pulses. *J Biomed Opt* 10(2):024001.
- Ng, E.Y.K. and E.H. Ooi. 2007. Ocular surface temperature: A 3D FEM prediction using bioheat equation. *Comput Biol Med* 37:829–835.
- Ooi, E.H. and E.Y.K. Ng. 2008. Simulation of aqueous humor hydrodynamics in human eye heat transfer. *Comput Biol Med* 38:252–262.
- Ooi, E.H., W.T. Ang and E.Y.K. Ng. 2008. A boundary element model of the human eye undergoing laser thermokeratoplasty. *Comput Biol Med* 38:727–737.
- Pflibsen, K.P., F.C. Delori, O. Pomerantzef and M.M. Pankratov. 1989. Fundus reflectometry for photocoagulation dosimetry. *Appl Opt* 28(6):1084–1096.
- Prydal, J.I. and F.W. Campbell. 1992. Study of precorneal tear film thickness and structure by interferometry and confocal microscopy. *Invest Ophthalmol Vis Sci* 33(6):1996–2005.

- Reddy, J.N. and D.K. Gartling. 2001. *The Finite Element Method in Heat Transfer and Fluid Dynamics*, 2nd edn. Boca Raton, FL: CRC.
- Rockwell, B.A., D. Hammer, P. Kennedy, et al. 1997. Retinal spot size with wavelength. In *Proceedings of SPIE, Laser-Tissue Interaction VIII*, ed. S.L. Jacques, SPIE Publishing, 2975:148–154.
- Roider, J. and R. Birngruber. 1995. Solution of the heat conduction equation. In *Optical-Thermal Response of Laser-Irradiated Tissue*, eds. A.J. Welch and M.J.C. van Gemert, pp. 385–409. New York: Plenum.
- Sanders, V.E. 1974. Wavelength dependence on threshold ocular damage from visible laser light. Report. Brooks City-Base, TX: USAF School of Aerospace Medicine.
- Sarna, T. 1992. Properties and functions of the ocular melanin: A photobiophysical view. *J Photochem Photobiol B* 12:215–258.
- Schüle, G., M. Rumohr, G. Huettmann and R. Brinkmann. 2005. RPE damage thresholds and mechanisms for laser exposure in the microsecond-to-millisecond time regimen. *Invest Ophthalmol Vis Sci* 46(2):714–719.
- Schulmeister, K., B.E. Stuck, D.J. Lund and D.H. Sliney. 2011. Review of thresholds and recommendations for revised exposure limits for laser and optical radiation for thermally induced retinal injury. *Health Phys* 100(2):210–220.
- Schulmeister, K., J. Husinsky, B. Seiser, F. Edthofer, H. Tuschl and D.J. Lund. 2006. Ex-plant retinal laser induced threshold studies in the millisecond time regime. In *Proceedings of SPIE, Optical Interactions with Tissue and Cells XVII*, eds. S.L. Jacques and W.P. Roach, SPIE Publishing, 6084.
- Scott, J. 1988. A finite element model of heat transport in the human eye. *Phys Med Biol* 33(2):227–241.
- Scott, J. 1988. The computation of temperature rises in the human eye induced by infrared radiation. *Phys Med Biol* 33(2):243–257.
- Segelstein, D.J. 1981. The complex refractive index of water. PhD. thesis, University of Missouri-Kansas City. Data compiled by S.A. Prahl. <http://omlc.ogi.edu/spectra/water/data/segelstein81.dat> (accessed March 28, 2011).
- Sliney, D.H. 2005. What is the minimal retinal image size?: Implications for setting MPEs. In *ILSC Proceedings*, Orlando, Florida, pp. 43–47.
- Sliney, D.H. and B.C. Freasier. 1973. Evaluation of optical radiation hazards. *Appl Opt* 12(1):1–24.
- Sliney, D.H., J. Mellerio, V.-P. Gabel and K. Schulmeister. 2002. What is the meaning of threshold in laser injury experiments? Implications for human exposure limits. *Health Phys* 82(3):335–347.
- Snodderly, D.M., G.J. Handelman and A.J. Adler. 1991. Distribution of individual macular pigment carotenoids in central retina of macaque and squirrel monkeys. *Invest Ophthalmol Vis Sci* 32(2):268–279.
- Snodderly, D.M., M.M. Sandstrom, I.Y.-F. Leung, C.I. Zucker and M. Neuringer. 2002. Retinal pigment epithelial cell distribution in central retina of Rhesus monkeys. *Invest Ophthalmol Vis Sci* 43(9):2815–2818.
- Spraul, C.W., G.E. Lang and H.E. Grossniklaus. 1996. Morphometric analysis of the choroid, Bruch's membrane and retinal pigment epithelium in eyes with age-related macular degeneration. *Invest Ophthalmol Vis Sci* 37(13):2724–2735.
- Stolarski, D.J., J. Stolarski, R.J. Thomas, G.D. Noojin, K.J. Schuster and B.A. Rockwell. 2002. Non-linear absorption studies of melanin. In *Proceedings of SPIE, Laser-Tissue Interaction XIII*, eds. S.L. Jacques et al., SPIE Publishing, 4617.
- Stuck, B.E. 1981. Ocular effects of holmium (2.06  $\mu\text{m}$ ) and erbium (1.54  $\mu\text{m}$ ) laser radiation. *Health Phys* 40:835–846.
- Takata, A.N., L.P. Kuan, L. Goldfinch, N. Thomopoulos, J.K. Hinds and A. Weigandt. 1974. Thermal model of laser-induced eye damage. Final report. Brooks City-Base, TX: USAF School of Aerospace Medicine.
- Thompson, C.R., B.S. Gerstman, S.L. Jacques and M.E. Rogers. 1996. Melanin granule model for laser-induced thermal damage in the retina. *Bull Math Biol* 58(3):513–553.
- van der Berg, T.J.T.P. and H. Spekreijse. 1997. Near infrared light absorption in the human eye. *Vision Res* 37(2):249–253.
- van Norren, D. and L.F. Tiemeijer. 1986. Spectral reflectance of the human eye. *Vision Res* 26(2):313–320.

- Verheyen, A. 1996. Necrosis and apoptosis: Irreversibility of cell damage and cell death. In *Toxicology: Principles and Applications*, eds. R.J.M. Niesink, J. De Vries and M.A. Hollinger, pp. 473–501. Boca Raton, FL: CRC.
- Vincelette, R.L., B.A. Rockwell, J.W. Oliver, et al. 2009. Trends in retinal damage thresholds from 100-millisecond near-infrared laser radiation exposures: A study at 1110, 1130, 1150 and 1319 nm. *Laser Surg Med* 41(5):382–390.
- Vogel, A. and R. Birngruber. 1992. Temperature profiles in human retina and choroid during laser coagulation with different wavelengths ranging from 514 to 810 nm. *Laser Light Ophthalmol* 5(1):9–16.
- Wang, Z., J. Dillon and E.R. Gaillard. 2006. Antioxidant properties of melanin in retinal pigment epithelial cells. *Photochem Photobiol* 82:474–479.
- Weiter, J.J., F.C. Delori, G.L. Wing and K.A. Fitch. 1986. Pigment epithelial lipofuscin and melanin and choroidal melanin in human eyes. *Invest Ophthalmol Vis Sci* 27(2):145–152.
- Welch, A.J. and G.D. Polhamus. 1984. Measurement and prediction of thermal injury in the retina of the Rhesus monkey. *IEEE Trans Biomed Eng* 31(10):633–644.
- Welch, A.J. and L.A. Priebe. 1980. Significance of blood flow in calculations of temperature in laser irradiated tissue. *IEEE Trans Biomed Eng* 27(3):164–166.
- Welch, A.J. and J.C. van Gemert. 1995. *Optical-Thermal Response of Laser-Irradiated Tissue*. New York: Plenum.
- Welch, A.J., L.A. Priebe, L.D. Forster, R. Gilbert, C. Lee and P. Drake. 1979. Experimental validation of thermal retinal models of damage from laser radiation. Final report. Brooks City-Base, TX: USAF School of Aerospace Medicine.
- Wikler, K.C. and P. Rakic. 1990. Distribution of photoreceptor subtypes in the retina of diurnal and nocturnal primates. *J Neurosci* 10(10):3390–3401.
- Wright, N.T. 2003. On a relationship between the Arrhenius parameters from thermal damage studies. *J Biomech Eng* 125:300–304.
- Zagers, N.P.A. and D. van Norren. 2004. Absorption of the eye lens and macular pigment derived from the reflectance of cone photoreceptors. *J Opt Soc Am A* 21(12):2257–2268.
- Zhang, R., W. Verkruyse, B. Choi, et al. 2005. Determination of human skin optical properties from spectrophotometric measurements based on optimization by genetic algorithms. *J Biomed Opt* 10(2):024030.
- Zuclich, J.A., H. Zwick, S.T. Schuscheraba, B.E. Stuck and F.E. Cheney. 1998. Ophthalmoscopic and pathologic description of ocular damage induced by infrared laser radiation. *J Laser Appl* 10(3):114–120.
- Zuclich, J.A., P. Edsall, D.J. Lund, et al. 2008. New data on the variation of laser induced retinal-damage threshold with retinal spot size. *J Laser Appl* 20(2):83–88.

